Amplitudes from eigenvalues

2012 Fluid Dyn. Res. 44 031202

(http://iopscience.iop.org/1873-7005/44/3/031202)

Fluid Dyn. Res. **44** (2012) 031202 (18pp) doi:10.1088/0169-5983/44/3/031202

REVIEW

Amplitudes from eigenvalues

Laurette S Tuckerman

PMMH (UMR 7636 CNRS–ESPCI–UPMC Univ Paris 06—UPD Univ Paris 07),
10 rue Vauquelin, 75005 Paris, France

E-mail: laurette@pmmh.espci.fr

Received 31 January 2012, in final form 26 March 2012
Published 2 May 2012
Online at stacks.iop.org/FDR/44/031202

Communicated by E Knobloch

Abstract
A dynamical system is generally understood first via linear stability analysis, which reduces to the diagonalization of a matrix, and then by studying the effects of the nonlinear terms. Surprisingly, in many cases of interest, the nonlinear analysis can also be reduced to the diagonalization of a matrix (similar to the linear stability matrix) whose eigenvalues yield nonlinear amplitudes. This provides a complementary alternative to the usual unfolding of codimension-two points or to the classification of dynamical systems by symmetry. Examples of such systems can be found in binary fluid convection and cylindrical or rotating convection.

1. Introduction

Many readers will have at least a passing familiarity with the title 'The unreasonable effectiveness of mathematics in the natural sciences' of the paper by Wigner (1960). Fluid dynamicists by now take for granted the astonishing effectiveness of dynamical-systems theory in modeling physical phenomena, relying, firstly, on the modeling of physical phenomena by differential equations and, secondly, on the usefulness of the dynamical-systems approach in understanding systems of differential equations. More specifically, we can note the success of low-dimensional dynamical systems theory, which can be attributed to the center manifold theorem and its generalizations, 'slaving' the many variables, which decay quickly to a few variables which are neutral, more slowly decaying or growing.

The archetypal systems that have been studied in this way, starting over a century ago, are the Taylor–Couette flow and Rayleigh–Bénard convection (e.g. Swinney and Gollub 1981). In idealized geometries, the basic state is known analytically and the linear stability of this state is determined by the eigenvalues of the Jacobian matrix. The nonlinear steady states must usually be calculated numerically, even for idealized cases. The numerically computed transitions in both idealized and realistic hydrodynamic pattern-forming systems can usually be interpreted as bifurcations in low-dimensional dynamical systems.

0169-5983/12/031202+18$33.00

For dynamical systems, the growth rate appears naturally as an eigenvalue in the linear stability problem. Eigenvalues can, however, appear in other contexts, with other meanings, for example as the forcing amplitude in the Faraday problem (Kumar and Tuckerman 1994). For certain dynamical systems, we have found that the nonlinear terms can be factored into a nonlinear scalar function (which we denote as an energy) and a linear operator. The value of this scalar function then appears in the steady-state equations as an eigenvalue. Moreover, for a given hydrodynamic configuration, the eigenproblem obeyed by the energy resembles that obeyed by the growth rates. We will explain the analogy between energy and growth rates that exists for a certain class of dynamical systems. This will be followed by two examples, both of which combine Rayleigh–Bénard convection with another effect: a concentration gradient (Tuckerman 2001) or differential rotation (Bordja *et al* 2010). Finally, we will discuss other special cases of low-dimensional dynamical systems (Gallet 2011), contrasting them with the exceptional nature of systems of eigenvalue type.

2. Linear stability and steady states

Consider a dynamical system of the form

$$\frac{\mathrm{d}}{\mathrm{d}t}\begin{pmatrix}A_1\\ \vdots\\ A_n\end{pmatrix} = \begin{pmatrix} & \mathcal{L} & \end{pmatrix}\begin{pmatrix}A_1\\ \vdots\\ A_n\end{pmatrix} - \mathcal{E}(A_1,\ldots,A_n)\begin{pmatrix} & \mathcal{M} & \end{pmatrix}\begin{pmatrix}A_1\\ \vdots\\ A_n\end{pmatrix} \tag{2.1}$$

where $\mathcal{L}$ and $\mathcal{M}$ are $n\times n$ matrices and $\mathcal{E}$ is a continuous function of $A_1,\ldots,A_n$. We specialize further to the case when $\mathcal{E}$ is a positive definite quadratic form, such as $A_1^2+\cdots+A_n^2$, invariant under the simultaneous change in sign of all A components, so that (2.1) is equivariant under the reflection $A\to -A$, where $A\equiv(A_1,\ldots,A_n)$. Moreover, we assume that both $\mathcal{L}$ and $\mathcal{M}$ are diagonalizable, and that $\mathcal{M}$ is invertible with positive real eigenvalues. By applying a similarity transformation, we take $\mathcal{M}$ diagonal.

We write (2.1) in the abbreviated form

$$\frac{\mathrm{d}}{\mathrm{d}t}A = \mathcal{L}A - \mathcal{E}(A)\,\mathcal{M}A. \tag{2.2}$$

The system (2.2) has a trivial solution $A=(0,0,\ldots,0)$, whose linear stability is controlled by the eigenvalues λ of $\mathcal{L}$:

$$\lambda A = \mathcal{L}A. \tag{2.3}$$

The steady states of (2.2) are solutions to

$$0 = \mathcal{L}A - \mathcal{E}(A)\,\mathcal{M}A, \tag{2.4}$$

that is,

$$EA = \mathcal{N}A, \tag{2.5}$$

where

$$\mathcal{E}(A) = E \tag{2.6}$$

and

$$\mathcal{N}\equiv\mathcal{M}^{-1}\mathcal{L}. \tag{2.7}$$

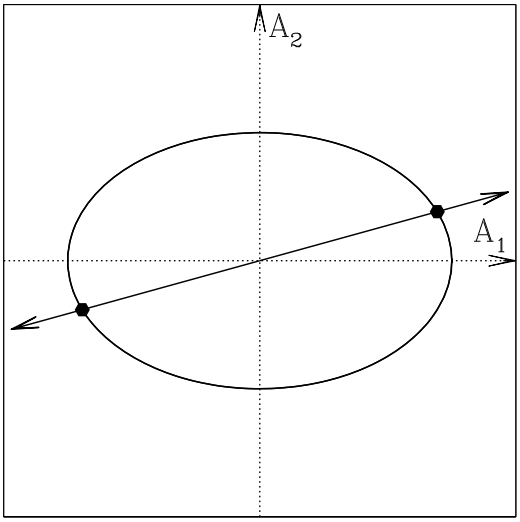

Figure 1. The elliptical curve represents $\mathcal{E}(A_1, A_2) = E$, while the arrows point in the direction of the corresponding eigenvector of $\mathcal{N}$. The intersections between the curve and the arrows are solutions to the nonlinear problem. For higher dimensions n, the curve would be an $(n-1)$-dimensional hypersurface.

Thus, for dynamical systems of the form (2.2), the steady states can be derived from an eigenvalue–eigenvector problem. For this reason, we refer to such systems as being of *eigenvalue type*. Equations (2.5) and (2.6) show that $\mathcal{E}(A)$ must be an eigenvalue of $\mathcal{N}$, with A being the corresponding eigenvector. Since $\mathcal{E}(A)$ is positive definite, only positive real values of E correspond to non-trivial steady states. (The trivial steady state also satisfies (2.5) and (2.6), with $A = 0$ and $E = 0$.) The requirement that A be an eigenvector fixes the relative amplitudes of the components of A, and the requirement that $\mathcal{E}(A) = E$ fixes its normalization, as illustrated in figure 1.

The interpretation of the eigenvalues λ of $\mathcal{L}$ of linear stability theory is well known. Real positive values of λ are associated with growing perturbations and real negative values with decaying perturbations. Complex eigenvalues λ are associated with oscillatory perturbations which also grow or decay, depending on the sign of the real part. A bifurcation occurs when the real part of λ crosses zero—a steady bifurcation if λ is real and a Hopf bifurcation if λ is complex. Because $\mathcal{E}$ is quadratic in A, the steady bifurcations are pitchforks, leading to steady states $\pm A$.

The interpretation of the eigenvalues E of $\mathcal{N}$ differs from that of the eigenvalues λ of $\mathcal{L}$ and is illustrated in figure 2. At a pitchfork bifurcation, E as well as λ changes sign; see figure 2(a), (b). This bifurcation-theoretic requirement is ensured by the fact that although $\mathcal{L}$ and $\mathcal{N}$ do not, in general, have the same eigenvalues or eigenvectors, a null vector of $\mathcal{L}$ must also be a null vector of $\mathcal{N} = \mathcal{M}^{-1}\mathcal{L}$. However, under the assumption that $\mathcal{E}$ is a non-negative real function, negative or complex eigenvalues E of $\mathcal{N}$ are meaningless. A saddle–node bifurcation occurs when two positive E values coalesce into a complex-conjugate pair, i.e. when two steady states join and cease to exist; see figure 2(c), (d). This event cannot be detected by any change in λ.

In spite of the very particular and restrictive form of (2.2), we have observed realizations of this duality between the linear and nonlinear problems in two physical systems. Both

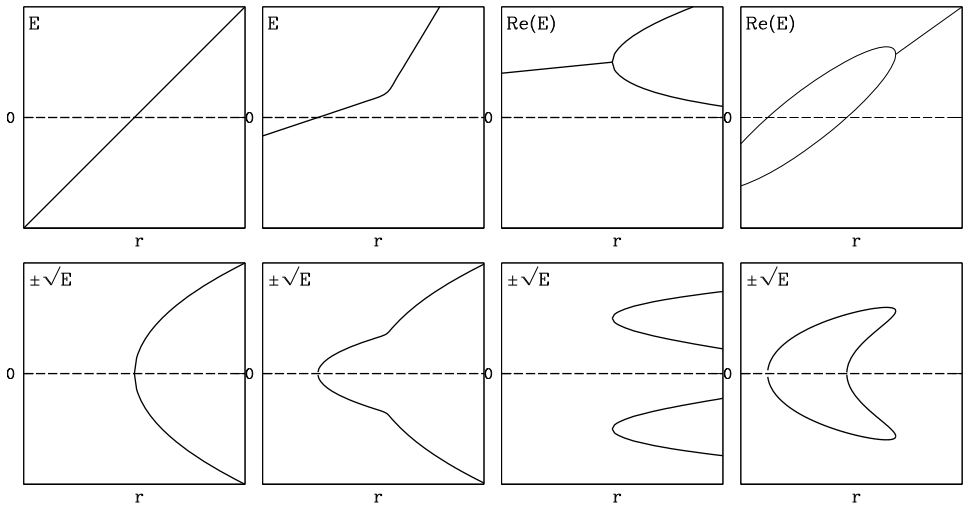

a) pitchfork *b) change of slope and curvature* *c) pair of saddle-nodes* *d) two pitchforks & pair of saddle-nodes*

Figure 2. Bifurcations corresponding to a qualitative change in E. $E = 0$ is always a solution and is shown as a dashed line. (a) E crosses zero at a critical value of r. At this value, two real non-zero values of $\pm\sqrt{E}$ appear, corresponding to a pitchfork bifurcation. (b) Following a pitchfork bifurcation, a change of slope in E leads to a change of curvature in $\pm\sqrt{E}$. This situation arises when two eigenvalues undergo avoided crossing rather than becoming complex conjugate pairs. (c) A pair of complex conjugate values of E becomes a pair of real values at a critical value of r. At this value, four real non-zero values of $\pm\sqrt{E}$ appear, corresponding to two saddle–node bifurcations. (d) Two real values of E successively become positive and then complex, corresponding to two pitchfork bifurcations, followed by a saddle–node bifurcation.

involve two variables, i.e.

$$\frac{\mathrm{d}}{\mathrm{d}t}\begin{pmatrix}A\\B\end{pmatrix} = \begin{pmatrix} \quad \mathcal{L} \quad \end{pmatrix}\begin{pmatrix}A\\B\end{pmatrix} - \mathcal{E}(A,B)\begin{pmatrix} \quad \mathcal{M} \quad \end{pmatrix}\begin{pmatrix}A\\B\end{pmatrix}. \tag{2.8}$$

Both describe the interaction between thermal convection and another instability mechanism in two spatial dimensions. These two systems have been studied in detail in previous publications (Tuckerman 2001, Bordja *et al* 2010). We summarize these two systems and their behavior below.

3. Binary fluids

A fluid mixture subjected to imposed vertical gradients of both temperature and concentration, in a two-dimensional geometry with free-slip horizontal and vertical boundary conditions, with the additional hypotheses of large Prandtl number and small amplitudes, is governed by the following dynamical system (Tuckerman 2001):

$$\frac{\mathrm{d}}{\mathrm{d}t}\begin{pmatrix}T\\C\end{pmatrix} = \begin{pmatrix} r-1 & Sr \\ r & Sr-L \end{pmatrix}\begin{pmatrix}T\\C\end{pmatrix} - \frac{1}{2}\left(\frac{rq}{2}\right)^2 (T+SC)^2 \begin{pmatrix}1 & 0\\ 0 & 1/L\end{pmatrix}\begin{pmatrix}T\\C\end{pmatrix}, \tag{3.1}$$

where T, C are deviations from linear temperature and concentration profiles, the Lewis number $L < 1$ is the ratio between thermal and solutal diffusivities, the separation parameter

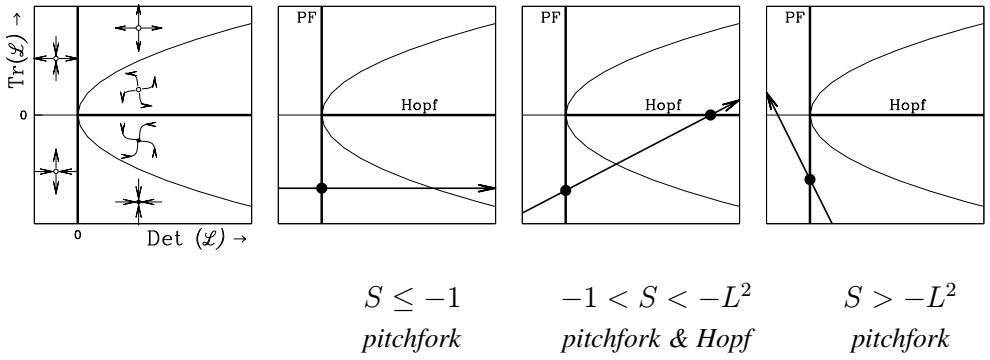

Figure 3. The eigenvalues of $\mathcal{L}$ determine the linear dynamics of the trivial steady state. The (Det($\mathcal{L}$),Tr($\mathcal{L}$)) plane is divided into regions in which eigenvalues are real or complex, with positive or negative real parts. The resulting dynamics are illustrated by phase portraits in the leftmost panel. An eigenvalue is zero along the line Det($\mathcal{L}$) = 0, corresponding to a pitchfork bifurcation. A complex eigenvalue has zero real part along the half-line Tr ($\mathcal{L}$) = 0, Det ($\mathcal{L}$) > 0, corresponding to a Hopf bifurcation. Arrows show paths as r is varied for three representative values of S; dots designate bifurcations undergone as the arrows cross the bifurcation lines. The TB codimension-two point is at the origin.

S is the ratio between solutal and thermal Rayleigh numbers, $q \equiv \pi\sqrt{3/2}$ is a geometric parameter and the reduced Rayleigh number r is the ratio of the Rayleigh number to the threshold for steady convection in the absence of a concentration gradient.

Bifurcations from the trivial state of (3.1) are determined by the eigenvalues λ of

$$\mathcal{L} = \begin{pmatrix} r-1 & Sr \\ r & Sr-L \end{pmatrix}, \tag{3.2}$$

where

$$\begin{aligned} \lambda_1 + \lambda_2 &= \mathrm{Tr}(\mathcal{L}) = (1+S)r - (1+L), \\ \lambda_1\lambda_2 &= \mathrm{Det}(\mathcal{L}) = -(S+L)r + L. \end{aligned} \tag{3.3}$$

A pitchfork bifurcation takes place when Det($\mathcal{L}$) = 0, while a Hopf bifurcation occurs when Det($\mathcal{L}$) > 0 and Tr($\mathcal{L}$) = 0, so that

$$\text{Pitchfork} \quad r_{\mathrm{PF}} = L/(S+L) \quad \text{for } S \neq -L, \tag{3.4a}$$

$$\text{Hopf} \quad r_{\mathrm{H}} = (1+L)/(1+S) \quad \text{for } -1 < S < -L^2. \tag{3.4b}$$

When Det($\mathcal{L}$) = Tr($\mathcal{L}$) = 0, the two thresholds coincide at the well-known Takens-Bogdanov codimension-two point:

$$r_* = \frac{1}{1-L}, \quad S_* = -L^2. \tag{3.5}$$

We will call this variously a TB, a PF/H or a linear codimension-two point, depending on the context. (Note that pitchfork and Hopf bifurcations may interact in other ways in systems with more variables; in such systems, the nomenclature PF/H would be ambiguous.) The trace and determinant of (3.2) as r and S are varied are illustrated in figure 3, along with the pitchfork and Hopf bifurcations encountered. The paths in the (Det, Tr) plane as r is varied, for fixed S, are straight lines; this is due to the linear dependence on r of (3.3).

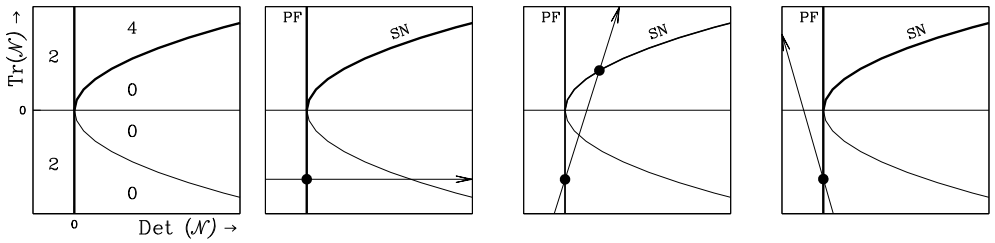

Figure 4. The eigenvalues of $\mathcal{N}$ determine the number of non-trivial steady states. The (Det($\mathcal{N}$), Tr($\mathcal{N}$)) plane is divided into regions in which there exist 0, 1 or 2 positive values of E and hence 0, 2 or 4 values of $\pm\sqrt{E}$, respectively, as shown in the leftmost panel. Two new values of $\pm\sqrt{E}$ appear or disappear when the line Det($\mathcal{N}$) = 0 is crossed, corresponding to a pitchfork bifurcation. Four new values of $\pm\sqrt{E}$ appear or disappear when crossing the curve Det ($\mathcal{N}$) = Tr ($\mathcal{N}$)^2/4, Tr ($\mathcal{N}$) > 0, corresponding to a pair of saddle–node bifurcations. The arrows show paths as r is varied for three representative values of S; the dots designate bifurcations undergone as the arrows cross the bifurcation lines. The degenerate pitchfork codimension-two point is at the origin.

Steady states of (3.1) are determined by the eigenvalues E of

$$\mathcal{N} = \mathcal{M}^{-1}\mathcal{L} = \begin{pmatrix} 1 & 0 \\ 0 & 1/L \end{pmatrix}^{-1} \begin{pmatrix} r-1 & Sr \\ r & Sr-L \end{pmatrix} = \begin{pmatrix} r-1 & Sr \\ Lr & LSr-L^2 \end{pmatrix} \quad (3.6)$$

with

$$\begin{aligned} E_1 + E_2 &= \mathrm{Tr}(\mathcal{N}) = (1+LS)r - (1+L^2), \\ E_1 E_2 &= \mathrm{Det}(\mathcal{N}) = -L(S+L)r + L^2. \end{aligned} \quad (3.7)$$

Specifically, a pair of steady states emerges from the pitchfork bifurcation, at which $\mathrm{Det}(\mathcal{N}) = \mathrm{Det}(\mathcal{M})^{-1}\mathrm{Det}(\mathcal{L}) = 0$, while two pairs of steady states emerge from a pair of saddle–node bifurcations when $\mathrm{Det}(\mathcal{N}) = \mathrm{Tr}(\mathcal{N})^2/4$ and $\mathrm{Tr}(\mathcal{N}) > 0$.

$$\text{Pitchfork} \quad r_{\mathrm{PF}} = L/(S+L) \quad \text{for } S \neq -L, \quad (3.8a)$$

$$\text{Saddle-node} \quad r_{\mathrm{SN}} = (1-L^2)/(1-\sqrt{-LS})^2 \quad \text{for } -L^{-1} < S < L^3. \quad (3.8b)$$

Another codimension-two point, at which pitchfork and saddle–node curves meet and the pitchfork changes from subcritical to supercritical, occurs when $\mathrm{Tr}(\mathcal{N}) = \mathrm{Det}(\mathcal{N}) = 0$:

$$\tilde{r}_* = \frac{1}{1-L^2}, \quad \tilde{S}_* = -L^3. \quad (3.9)$$

We will call this a degenerate pitchfork, a PF/SN or a nonlinear codimension-two point. The trace and determinant (3.7) as r and S are varied are illustrated in figure 4, along with the pitchfork and saddle–node bifurcations encountered.

The bifurcations of (3.1) in the (S, r) plane for $S < 0$ are summarized in figure 5. The system (3.1) contains a number of other bifurcations, in particular a heteroclinic bifurcation at which the limit cycle created by the Hopf bifurcation is destroyed by colliding with two saddle points. The analysis of the curves emanating from the TB codimension-two point is well documented by, e.g., Knobloch and Proctor (1981), Arnold (1982), Knobloch (1986) and Kuznetsov (1998). We will not cover this topic because our focus is on the resemblance of the linear and nonlinear problems. The dynamics of the model system (3.1), studied in detail

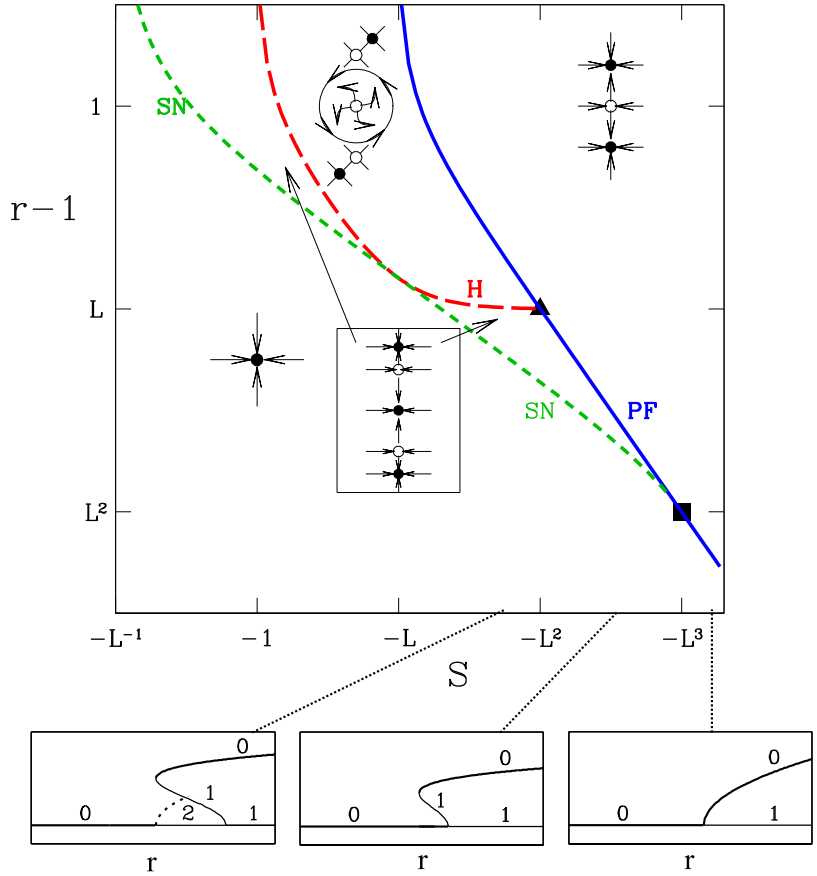

Figure 5. Top: the bifurcation set of the thermosolutal problem for $S < 0$ with representative phase portraits. Curves of pitchfork, saddle–node and Hopf bifurcations are indicated by blue solid, green short-dashed and red long-dashed curves. Pitchfork and Hopf bifurcation curves meet at the linear (Takens–Bogdanov) codimension-two point indicated by the triangle at $S_* = -L^2$, $r_* = 1/(1-L) \approx 1+L$. Pitchfork and saddle-node bifurcation curves meet at the nonlinear (degenerate pitchfork) codimension-two point indicated by the square at $\tilde{S}_* = -L^3$, $\tilde{r}_* = 1/(1-L^2) \approx 1+L^2$. The curve of global (heteroclinic) bifurcations annihilating the limit cycle and emanating from the TB point is not shown. Hopf and saddle–node bifurcations do not interact, so the intersection of the corresponding curves does not give rise to any special dynamics. Bottom: representative bifurcation diagrams for fixed S in the ranges indicated showing steady states (solid curves) and limit cycles (dotted curves). Numbers along steady state branches indicate the number of unstable eigenvalues, i.e. 0 indicates a stable branch, while 1 and 2 indicate branches with one and two unstable eigenvalues.

in Tuckerman (2001), greatly resembles that of fully resolved 2D numerical simulations of, for example, binary fluid convection with the Soret effect (Knobloch 1986, Hollinger *et al* 1998), double-diffusive convection (Da Costa *et al* 1981) or Marangoni (surface-tension-driven) convection in a mixture (Bergeon *et al* 1988).

4. Convection in a cylinder with counter-rotating discs

A fluid in a cylindrical container is subjected to an imposed vertical temperature gradient by differentially heating the top and bottom bounding discs and simultaneously to an imposed

angular velocity gradient by differentially rotating the bounding discs. This configuration is called the Rayleigh–Bénard–von Kármán (RBVK) problem. Restricting consideration to the axisymmetric solutions in a cylinder of equal radius and height, this flow will undergo a pitchfork bifurcation if the differential rotation is low or a Hopf bifurcation if it is high (Bordja *et al* 2010). The differences between the angular velocities and temperature of the upper and lower discs are measured by the Reynolds and Rayleigh numbers, respectively; the behavior over the (Reynolds, Rayleigh) plane is shown in figure 6.

This case differs in a number of ways from the thermosolutal system studied in the previous section. In (3.1), the two components T and C are associated with different physical phenomena but the same geometric form. In contrast, numerical investigation of the full RBVK equations (Bordja *et al* 2010) shows that the two interacting modes differ geometrically: one contains a single toroidal roll and the other contains two concentric toroidal rolls.

A dynamical system that captures many of these phenomena is given by

$$\frac{\mathrm{d}}{\mathrm{d}t}\begin{pmatrix} A \\ B \end{pmatrix} = \underbrace{\begin{pmatrix} r+1 & \Omega^2 \\ -\Omega^2 & r-1 \end{pmatrix}}_{\mathcal{L}}\begin{pmatrix} A \\ B \end{pmatrix} - \mathcal{E}(A,B)\underbrace{\begin{pmatrix} 1 & 0 \\ 0 & 1 \end{pmatrix}}_{\mathcal{M}}\begin{pmatrix} A \\ B \end{pmatrix} \tag{4.1}$$

with $\mathcal{E}(A, B)$ being an unspecified positive definite quadratic form. Unlike (3.1), the model system (4.1) is not derived from the underlying full hydrodynamic equations. The behavior of the system (4.1) as a function of r and Ω is illustrated in figure 7; a similar figure is found in Gallet (2011). Since $\mathcal{M} = I$, we have $\mathcal{N} = \mathcal{L}$, whose eigenvalues are

$$\lambda = E = \frac{\mathrm{Tr}(\mathcal{L})}{2} \pm \sqrt{\left(\frac{\mathrm{Tr}(\mathcal{L})}{2}\right)^2 - \mathrm{Det}(\mathcal{L})} = r \pm \sqrt{1-\Omega^4}. \tag{4.2}$$

These eigenvalues determine the pitchfork and Hopf bifurcations, as well as the saddle–node bifurcations. A pitchfork bifurcation occurs when $\mathrm{Det}(\mathcal{L}) = 0$, a Hopf bifurcation when $\mathrm{Det}(\mathcal{L}) > 0$, and $\mathrm{Tr}(\mathcal{L}) = 0$, and a saddle–node bifurcation when $\mathrm{Det}(\mathcal{L}) = \mathrm{Tr}(\mathcal{L})^2/4$ and $\mathrm{Tr}(\mathcal{L}) > 0$.

$$\text{Pitchfork} \quad r_{\mathrm{PF}} = \pm\sqrt{1-\Omega^4} \quad \text{for } \Omega \leqslant 1, \tag{4.3a}$$

$$\text{Hopf} \quad r_{\mathrm{H}} = 0 \quad \text{for } \Omega > 1, \tag{4.3b}$$

$$\text{Saddle–node} \quad \Omega_{\mathrm{SN}} = 1 \quad \text{for } r > 0. \tag{4.3c}$$

All three bifurcation curves meet when $\mathrm{Tr}(\mathcal{L}) = \mathrm{Det}(\mathcal{L}) = 0$:

$$r_* = 0, \quad \Omega_* = 1 \tag{4.4}$$

This is a codimension-three point, which has been studied extensively along with its unfolding by Dumortier *et al* (1991). It is natural for the case $\mathcal{M} = I$ to lead to codimension-three points, since the linear and nonlinear codimension-two points are then identical.

The actual RBVK problem, as shown in figure 6, does not contain a codimension-three point, but rather two codimension-two points (PF/H and PF/SN). The same juxtaposition of codimension-two points as in the RBVK scenario has been observed in numerical simulations of double-diffusive convection in a 2D rectangular container (Meca *et al* 2004). A more

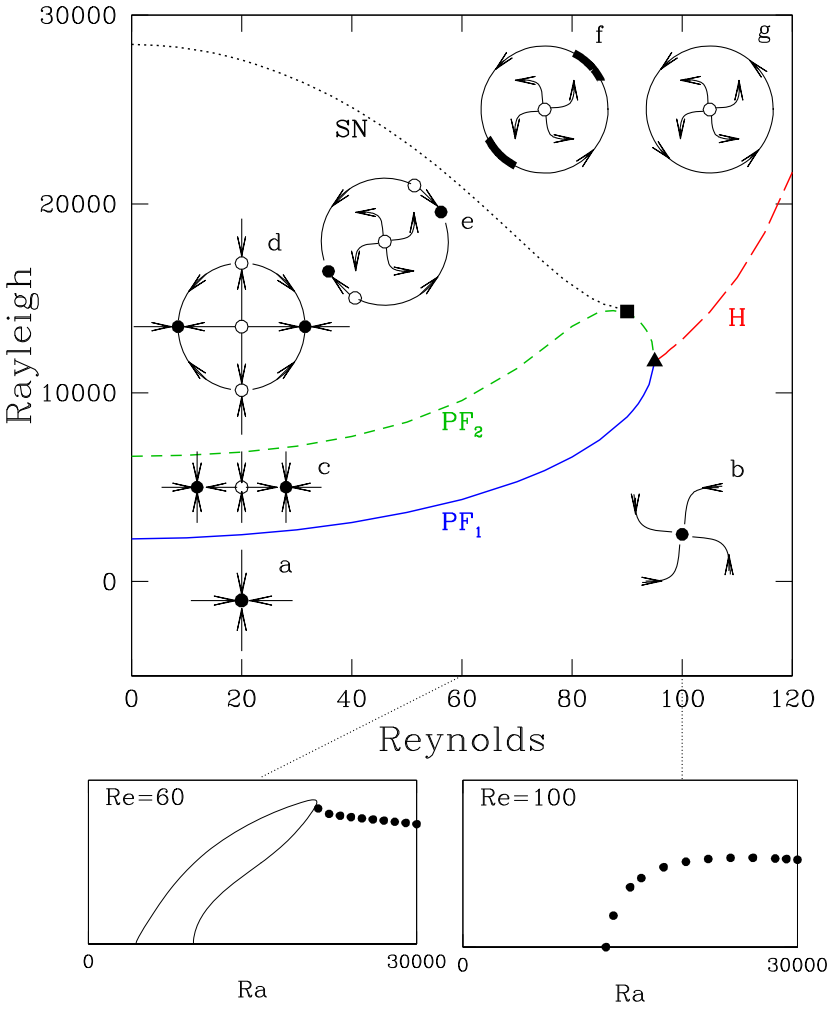

Figure 6. Top: numerically computed curves of bifurcation points for the RBVK problem in the (Re, Ra) plane showing the first pitchfork (blue, solid, PF_1), second pitchfork (green, short dashed, PF_2), Hopf (red, long dashed, H) and saddle–node (black, dotted, SN) bifurcations. Dots indicate codimension-two points, where the curve PF_2 meets curves H (triangle, TB) and SN (square). Phase portraits shown as insets. (a, b) Below PF_1 and H, the only solution is the stable basic flow, which is a node (a) or a spiral focus (b). (c) Between PF_1 and PF_2, the basic flow is unstable and there exist two stable asymmetric convective states. (d, e) Between PF_2 and SN, there exist five states: the unstable basic flow and two stable and two unstable convective states. (f, g) Between SN and H, the unstable basic flow is surrounded by a stable limit cycle, which is near-heteroclinic near SN (f) and near-sinusoidal near H (g). Other bifurcation curves (a saddle–node of periodic orbits, a gluing bifurcation and a secondary Hopf bifurcation) emanating from the TB point are not shown here; see Bordja *et al* (2010). Bottom: bifurcation diagrams. For $Re = 60$, two pairs of steady branches appear via successive pitchforks and disappear via a pair of sniper bifurcations leading to a limit cycle. For $Re = 100$, a limit cycle is created by a Hopf bifurcation.

faithful model of this scenario can be obtained by taking $\mathcal{M} \neq I$:

$$\frac{\mathrm{d}}{\mathrm{d}t}\begin{pmatrix} A \\ B \end{pmatrix} = \underbrace{\begin{pmatrix} r+1 & \Omega^2 \\ -\Omega^2 & r-1 \end{pmatrix}}_{\mathcal{L}}\begin{pmatrix} A \\ B \end{pmatrix} - \mathcal{E}(A,B)\underbrace{\begin{pmatrix} 1 & 0 \\ 0 & \delta \end{pmatrix}}_{\mathcal{M}}\begin{pmatrix} A \\ B \end{pmatrix}. \tag{4.5}$$

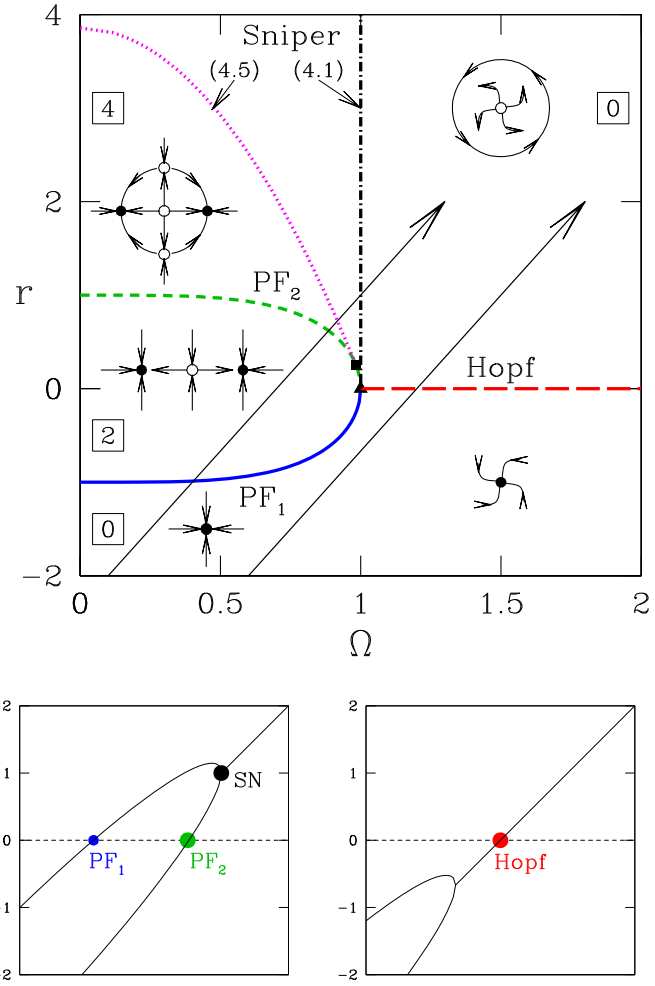

Figure 7. Top: curves of bifurcation points in the (Ω, r) plane of the system (4.1) or (4.5) with $\delta = 0.59$ showing PF_1 (blue, solid), PF_2 (green, short-dashed) and Hopf (red, long-dashed) bifurcations. For the model (4.1), the sniper bifurcation curve (black, dash-dotted) meets the PF and Hopf curves at a single codimension-three point (solid triangle). In contrast, for the model (4.5), the sniper bifurcation curve (magenta, dotted) meets the PF_2 curve in a PF/SN codimension-two point (solid square) and the meeting of the PF and Hopf curves (solid triangle) becomes a PF/H codimension-two point. The arrows indicate two paths through the (Ω, r) plane. The bifurcations encountered are either a Hopf bifurcation or else two pitchforks and one sniper bifurcation. As in figure 6, several other bifurcation curves emerge from the TB point, but are not shown here. Each sector contains a phase portrait and a number (0, 2, 4) within a square, which counts the number of non-trivial steady solutions. Below: eigenvalues λ or energy E along two paths, one through the two pitchforks and sniper bifurcation, and the other through the Hopf bifurcation.

For simplicity, δ is assumed to be independent of r and Ω. The pitchfork and Hopf bifurcation curves remain unchanged, but the saddle–node bifurcations take place at

$$\Omega_{SN}^2 = \frac{r(\delta - 1) + (\delta + 1)}{2\sqrt{\delta}} \tag{4.6}$$

and the PF/SN codimension-two point is located at

$$\tilde{r}_* = \frac{1-\delta}{1+\delta}, \qquad \tilde{\Omega}_*^2 = \sqrt{1-\tilde{r}_*^2} = \frac{2\sqrt{\delta}}{1+\delta}. \tag{4.7}$$

The bifurcation curves for system (4.1) and for system (4.5) are shown in figure 7.

As in the thermosolutal case of (3.1), the limit cycles produced by the Hopf bifurcation in (4.3*b*) can also be destroyed by some other bifurcation. In the thermosolutal case, this occurs via a heteroclinic cycle, present in (3.1) but not detectable via the eigenvalues λ or E. In system (4.1), however, the limit cycles are destroyed by the saddle–node bifurcations (4.3*c*). Therefore, their termination is manifested as changes in E. This is illustrated by the phase portaits in figure 6. Saddle–node bifurcations under these circumstances are called SNIPER (Saddle–Node-Infinite-PERiod), SNIC (Saddle–Node on invariant circle) or Andronov bifurcations (Andronov and Leontovich 1939, Kuznetsov 1998).

SNIPER bifurcations should be ubiquitous in the symmetric hydrodynamic systems for the following reasons. Two sequential pitchfork bifurcations lead naturally to a ring of alternating stable and unstable fixed points, all located on an invariant manifold. As parameters are varied, it is natural for these fixed points to approach one another along the invariant manifold, leading eventually to a sniper bifurcation. SNIPER bifurcations are indeed quite common and have been observed, e.g. in axisymmetric modulated rotating convection (Lopez *et al* 2006, Rubio *et al* 2008) and in non-axisymmetric small-aspect-ratio Taylor–Couette flow (Abshagen *et al* 2005a,b). A sniper bifurcation has been proposed as a possible explanation for reversals of the magnetic fields of celestial bodies (Pétrélis *et al* 2009, Gallet 2011).

However, scenarios involving consecutive pitchfork bifurcations may play out in different ways. Axisymmetric convection provides a good illustration of when sniper bifurcations may or may not be observed. Simulations (Tuckerman and Barkley 1988) in a cylinder of radius-to-height aspect ratio 5 with conducting sidewalls have shown a sniper bifurcation in which a set of concentric rolls begin to drift radially. For insulating sidewalls, the evolution is instead to other steady states produced via an additional pair of saddle–node bifurcations (Barkley and Tuckerman 1989). When the sidewalls and the upper and lower bounding discs are taken to be stress free and the aspect ratio is between 6.6 and 10, a completely different scenario is observed (Siggers 2003). Consecutive pitchfork bifurcations still lead to steady states that annihilate one another via saddle–node bifurcations, but the transition scenario actually realized includes heteroclinic, homoclinic and gluing bifurcations rather than sniper bifurcations. (We recall that other bifurcation curves are present in systems (4.1) and (4.5) and in figures 6 and 7 but do not play an important role.) The analysis of a system of eigenvalue type can predict the presence of saddle–node bifurcations, but not whether these lead to limit cycles.

corrected (5) from published version

The next section discusses the relationship between saddle–node bifurcations and symmetry, in particular the conditions under which symmetry may suppress saddle–node bifurcations.

5. Symmetry

The evolution of a system that has undergone two simultaneous or sequential pitchfork bifurcations may be such that the fixed points never meet. An important factor in deciding whether or not they meet is symmetry. The classification of dynamical systems by their symmetry has been studied extensively; see, for example, Hirschberg and Knobloch (1997) and Gallet (2011). In table 1, we set out a hierarchy of two-variable dynamical systems

Table 1. Rotational symmetries, names of symmetry groups, corresponding dynamical systems, and steady states for the reflection-symmetric case. Systems with reflection symmetry ($z \to \bar{z}$) have real coefficients; those without have complex coefficients.

Rotations	Reflection		Dynamical system	
	with	without	Steady states	
All θ	$O(2)$	$SO(2)$	$\dot{z} = \mu z - b\lvert z\rvert^2 z$	
			$R^2 = \mu/b$	θ arbitrary
$j\pi/2$	D_4	Z_4	$\dot{z} = \mu z - (b\lvert z\rvert^2 z + d\bar{z}^3)$	
			$R^2 = \mu/(b+d)$	$\theta = j\pi/2$
			$R^2 = \mu/(b-d)$	$\theta = j\pi/2 + \pi/4$
$j\pi$	D_2	Z_2	$\dot{z} = \mu z + \nu\bar{z} - (az^3 + b\lvert z\rvert^2 z + cz\bar{z}^2 + d\bar{z}^3)$	
			$R^2 = (\mu+\nu)/(a+b+c+d)$	$\theta = j\pi$
			$R^2 = (\mu-\nu)/(-a+b-c+d)$	$\theta = j\pi + \pi/2$
			$R^2 = \frac{d\mu-\nu a}{d(b-d)+a(a-c)}$	$\cos 2\theta = \frac{\nu(b-d)+\mu(a-c)}{2(d\mu-\nu a)}$

with decreasing symmetry. The dynamical systems are written in terms of a single complex variable z describing the amplitudes of the bifurcating modes. All of the systems have the reflection symmetry $z \to -z$. Systems with the additional reflection symmetry $z \to \bar{z}$ have real coefficients and those without have complex coefficients. Coefficients such as μ are assumed to be real unless subscripts are specified, e.g. μ_r, μ_i.

Steady solutions, where they exist, are also listed in table 1. These are most easily calculated by setting $z = R\,\mathrm{e}^{\mathrm{i}\theta}$. For the D_2 case, for example, we have

$$\dot{z} = (\dot{R} + \mathrm{i}\dot{\theta}R)\mathrm{e}^{\mathrm{i}\theta} = R(\mu\,\mathrm{e}^{\mathrm{i}\theta} + \nu\,\mathrm{e}^{-\mathrm{i}\theta}) - R^3(a\,\mathrm{e}^{3\mathrm{i}\theta} + b\,\mathrm{e}^{\mathrm{i}\theta} + c\,\mathrm{e}^{-\mathrm{i}\theta} + d\,\mathrm{e}^{-3\mathrm{i}\theta}), \tag{5.1}$$

leading to equations for R and θ:

$$0 = \dot{R} = R(\mu + \nu\cos(2\theta)) - R^3(a\cos(2\theta) + b + c\cos(2\theta) + d\cos(4\theta)), \tag{5.2a}$$

$$0 = \dot{\theta} = -\nu\sin(2\theta) - R^2(a\sin(2\theta) - c\sin(2\theta) - d\sin(4\theta)). \tag{5.2b}$$

Figure 8 shows the behavior that commonly occurs in systems with different symmetries. In the $O(2)$ system, the two eigenmodes are basis vectors of a single eigenspace; a circle pitchfork bifurcation creates a circle of steady states. For D_4 systems, the parameter d introduces inhomogeneity in θ and thus preferred phases. Such a system bifurcates simultaneously to eight nonlinear states, divided into two non-equivalent classes. These equations arise in convection in square systems, where four branches correspond to vertical and horizontal directions and four to diagonal directions (Bergeon *et al* 2001). (The same equations arise when a Hopf bifurcation breaks $O(2)$ symmetry, creating branches of standing and traveling waves (Swift 1984).) For D_2 systems, the parameter ν separates the thresholds for the two modes, and so these systems undergo two consecutive pitchfork bifurcations. The resulting states can in turn undergo secondary pitchfork bifurcations to mixed-mode states (e.g. Knobloch and Guckenheimer 1983, Hirschberg and Knobloch 1997). Examples are the Eckhaus instability (Tuckerman and Barkley 1990) and the 3D instability of the wake behind a cylinder (Barkley *et al* 2000). For Z_2 systems, the parameter μ_i introduces complex eigenvalues, allowing the systems to undergo Hopf bifurcations. This parameter also allows pairs of steady states to join and annihilate one another in saddle–node (sniper) bifurcations. It is precisely these two phenomena that are connected by our eigenvalue analysis.

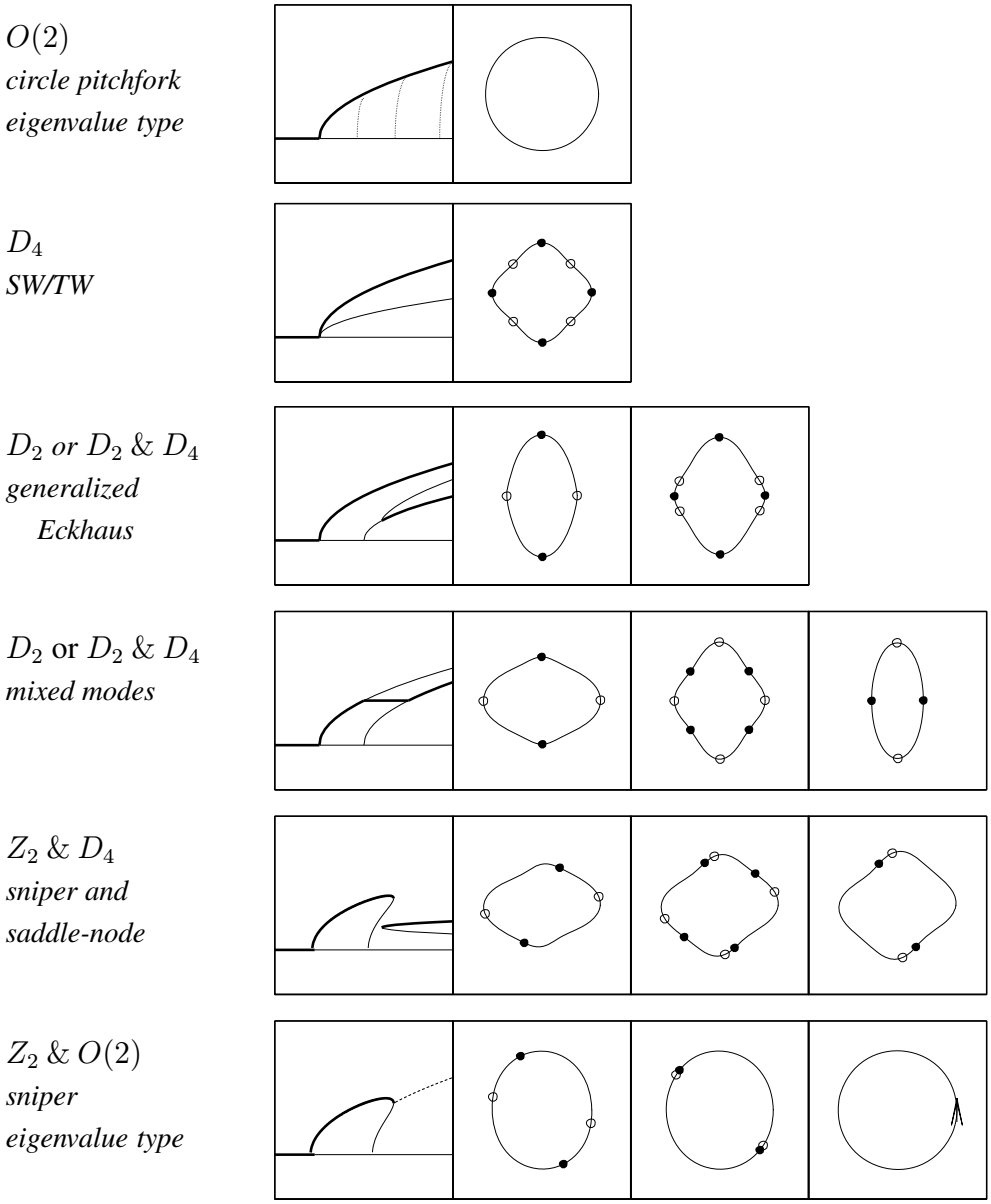

Figure 8. Representative bifurcation diagrams and phase portraits for dynamical systems with symmetries as indicated. The notation $O(2)$, for example, means that the linear and nonlinear terms have symmetry $O(2)$, while $Z_2\&O(2)$ means that the linear terms have Z_2 symmetry and the nonlinear terms have $O(2)$ symmetry; see text. Stable (unstable) branches are shown as thick (thin) curves, while stable (unstable) steady states are shown as solid (hollow) dots. The limit cycle emerging from the sniper bifurcation in the last row is shown as a dashed curve. In the phase portraits, the curves shown are those on which $\dot{R} = 0$, which resemble but are not identical to the trajectories connecting the steady states.

As the system becomes less symmetric, its general form becomes less restrictive and therefore more complicated; in particular, the Z_2 form has four complex or eight real nonlinear coefficients. For this reason, researchers, e.g. Hirschberg and Knobloch (1997),

Bergeon *et al* (2001) and Gallet (2011), have proposed various hybrid forms in which the symmetry is broken only in the linear terms and retained in the nonlinear terms. The reasoning behind this is that if the symmetry breaking is weak, then its effect on the nonlinear terms will be negligible compared to that on the linear terms.

Hirschberg and Knobloch (1997) have systematically derived systems which describe the competition between neighboring wavenumbers in a wide 2D container, with various horizontal boundary conditions. For a container of finite width, the system is described by equations with D_2 symmetry. However, in the limit of infinite width, containers with free-slip or no-slip boundaries lead to D_4 or $O(2)$ symmetry, respectively. Hirschberg and Knobloch therefore propose systems in which the linear terms have the D_2 symmetry appropriate for the finite width and the nonlinear terms have either D_4 or $O(2)$ symmetry, appropriate for infinite width. We denote these systems as having $D_2\&D_4$ or $D_2\&O(2)$ symmetry. Bergeon *et al* (2001) have also used $D_2\&D_4$ symmetric equations to describe 3D Marangoni convection in containers with a nearly square cross-section.

Turning to systems containing a Hopf bifurcation, Gallet (2011) has proposed a system of hybrid symmetry to describe the competition between dynamos of quadrupole or dipole form as well as the competition between neighboring wavenumbers in a wide 2D container with weakly broken reflection symmetry. The linear terms have Z_2 symmetry (i.e. μ and ν are complex), while the nonlinear terms have D_4 symmetry (i.e. there are two real nonlinear coefficients, b and d). This dynamical system, whose symmetry we can characterize as $Z_2\&D_4$, is

$$Z_2\,\&\,D_4: \quad \dot z = (\mu_r + \mathrm{i}\mu_i)z + (\nu_r + \mathrm{i}\nu_i)\bar z - bz^2\bar z - d\bar z^3, \tag{5.3}$$

$$\frac{\mathrm{d}}{\mathrm{d}t}\begin{pmatrix} x \\ y \end{pmatrix} = \begin{pmatrix} \mu_r + \nu_r & -\mu_i + \nu_i \\ \mu_i + \nu_i & \mu_r - \nu_r \end{pmatrix}\begin{pmatrix} x \\ y \end{pmatrix} - \begin{pmatrix} x(b(x^2+y^2) + d(x^2-3y^2)) \\ y(b(x^2+y^2) + d(y^2-3x^2)) \end{pmatrix}.$$

The presence of the term $d\bar z^3$ in (5.3) has several consequences. System (5.3) is not of the eigenvalue type unless $d = 0$. Moreover, equations (5.2*a*) and (5.2*b*) show that this term can lead to the existence of eight non-trivial steady states.

Systems whose nonlinear terms have $SO(2)$ symmetry have been used to model time-dependent convection (Riecke *et al* 1988, Siggers 2003). The general form of such a system is

$$Z_2\,\&\,SO(2): \quad \dot z = (\mu_r + i\mu_i)z + (\nu_r + i\nu_i)\bar z - (b_r + \mathrm{i}b_i)|z|^2 z, \tag{5.4}$$

$$\frac{\mathrm{d}}{\mathrm{d}t}\begin{pmatrix} x \\ y \end{pmatrix} = \begin{pmatrix} \mu_r + \nu_r & -\mu_i + \nu_i \\ \mu_i + \nu_i & \mu_r - \nu_r \end{pmatrix}\begin{pmatrix} x \\ y \end{pmatrix} - (x^2+y^2)\begin{pmatrix} b_r & -b_i \\ b_i & b_r \end{pmatrix}\begin{pmatrix} x \\ y \end{pmatrix}.$$

With $\nu = 1$ and $b = 1 - 0.8i$, Siggers (2003) has reproduced a transition from radial convection rolls to radially travelling waves that includes heteroclinic, homoclinic and gluing bifurcations. The $SO(2)$ symmetry of the nonlinear terms can be understood as meaning that they distinguish between the inwards and outwards radial directions, but not between different radial locations. System (5.4) satisfies a generalization of our definition of systems of eigenvalue form, since its nonlinear term is a product of a quadratic function with a matrix–vector product, but the matrix does not have positive real eigenvalues.

We now turn to the models studied in section 4. The examples we have given of sniper bifurcations are in axisymmetric cylindrical systems and involve competition between wavelengths in the radial direction. These examples can be considered as perturbed versions of systems with $O(2)$ symmetry: the radial direction has some remnant of both translational and

reflectional symmetry. (The remaining unbroken Z_2 symmetry is the Boussinesq symmetry combining temperature reversal with vertical reflection, which is unaffected by changes in the horizontal geometry.) Equation (4.1), a system of the eigenvalue type used to model the RBVK system in the previous section, combines Z_2 symmetry for the linear terms with $O(2)$ symmetry for the nonlinear terms. The general form for such a system is

$$Z_2 \,\&\, O(2): \quad \dot{z} = (\mu_r + i\mu_i)z + (\nu_r + \mathrm{i}\nu_i)\bar{z} - b|z|^2 z, \tag{5.5}$$

$$\frac{\mathrm{d}}{\mathrm{d}t}\begin{pmatrix} x \\ y \end{pmatrix} = \begin{pmatrix} \mu_r + \nu_r & -\mu_i + \nu_i \\ \mu_i + \nu_i & \mu_r - \nu_r \end{pmatrix}\begin{pmatrix} x \\ y \end{pmatrix} - (x^2 + y^2)\begin{pmatrix} b & 0 \\ 0 & b \end{pmatrix}\begin{pmatrix} x \\ y \end{pmatrix}.$$

In order to unfold the codimension-three point of (4.1), we introduced another system of eigenvalue type, (4.5), whose general form can be written as

$$Z_2: \quad \dot{z} = (\mu_r + \mathrm{i}\mu_i)z + (\nu_r + \mathrm{i}\nu_i)\bar{z} - (b|z|^2 z + c|z|^2\bar{z}), \tag{5.6}$$

$$\frac{\mathrm{d}}{\mathrm{d}t}\begin{pmatrix} x \\ y \end{pmatrix} = \begin{pmatrix} \mu_r + \nu_r & -\mu_i + \nu_i \\ \mu_i + \nu_i & \mu_r - \nu_r \end{pmatrix}\begin{pmatrix} x \\ y \end{pmatrix} - (x^2 + y^2)\begin{pmatrix} b+c & 0 \\ 0 & b-c \end{pmatrix}\begin{pmatrix} x \\ y \end{pmatrix}.$$

This system has no overall symmetry beyond Z_2.

We can contrast the dynamical systems obtained by symmetry considerations with those of eigenvalue type. Both apply certain hypotheses in order to reduce the number of nonlinear terms to a more manageable set. These hypotheses are not the same and lead to different results. Systems (5.3), (5.4) and (5.6) are all generalizations of (5.5) and all contain two nonlinear parameters, but they have fundamentally different properties. An important consideration is the number of steady states. A two-variable system of eigenvalue type cannot have more than four non-trivial states, since 2×2 matrices have at most two real eigenvalues, which in turn have at most four square roots. (It is possible that this restriction can be relaxed and the maximum number of states increased by generalizing the scalar function $\mathcal{E}$ beyond the current requirement that it be a positive definite quadratic form.) In contrast, the maximum number of nontrivial solutions of a two-variable system of cubic order is $3^2 - 1 = 8$, since a system of n equations in n variables each of order j has at most j^n solutions.

Gallet (2011) showed that system (5.3) is able to produce not only sniper and Hopf bifurcations, such as (4.1) and (4.5), but the full range of phenomena produced by wavelength competition. These include mixed-mode states created by secondary pitchfork bifurcations, i.e. generalized Eckhaus bifurcations (Tuckerman and Barkley 1990), mixed modes (Barkley *et al* 2000), as well as additional saddle–node bifurcations (Barkley and Tuckerman 1989). These scenarios, illustrated by rows 3–5 of figure 8, produce eight nontrivial steady states and so cannot be captured by a system of eigenvalue type such as (4.1) or (4.5).

More philosophically, the approach of deriving equations based on weakly broken symmetry can and has been amply justified theoretically. In contrast, systems of eigenvalue type are inspired by observations of resemblance between linear and nonlinear behaviors, more specifically between the eigenvalues of the linear system and the non-trivial steady states, which are usually thought to be unrelated.

6. Discussion

Sections 3 and 4 have shown that a number of hydrodynamic configurations behave like dynamical systems of eigenvalue type. However, most dynamical systems are not of the eigenvalue form (2.2). In fact, even most two-variable systems with cubic nonlinearities are

not of this type. We write

$$\begin{pmatrix} c_0A^3+c_1A^2B+c_2AB^2+c_3B^3 \\ d_3A^3+d_2A^2B+d_1AB^2+d_0B^3 \end{pmatrix} = \mathcal{E}\underbrace{\begin{pmatrix} \alpha & \beta \\ \gamma & \delta \end{pmatrix}}_{\mathcal{M}}\begin{pmatrix} A \\ B \end{pmatrix}, \tag{6.1}$$

where the eight coefficients $c_0,\ldots,c_3,d_3,\ldots,d_0$ are linear combinations of the coefficients $a_r,\ldots,d_r,a_i,\ldots,d_i$ mentioned in table 1. Setting

$$\frac{c_0A^3+c_1A^2B+c_2AB^2+c_3B^3}{\alpha A+\beta B} = \mathcal{E} = \frac{d_3A^3+d_2A^2B+d_1AB^2+d_0B^3}{\gamma A+\delta B} \tag{6.2}$$

and cross-multiplying leads to an equation in the five fourth-order monomials A^jB^{4-j}. Separating the monomials leads to a system of five linear homogeneous equations in the four elements $\alpha,\beta,\gamma,\delta$ of $\mathcal{M}$. The existence of a nontrivial solution requires the eight nonlinear coefficients $c_0,\ldots,d_0$ to satisfy two equations. (Note that satisfying four linear homogeneous equations would lead to the single condition that the determinant be zero.) Additional inequalities must be satisfied in order for $\mathcal{M}$ to have real eigenvalues and for $\mathcal{E}$ to be positive definite.

Conversely, if we start by supposing that, in (6.1), $\mathcal{M}$ has been diagonalized and scaled so that

$$\mathcal{M} = \begin{pmatrix} 1 & 0 \\ 0 & \delta \end{pmatrix}, \tag{6.3}$$

then it is easy to show that

$$\frac{d_2}{c_0} = \frac{d_1}{c_1} = \frac{d_0}{c_2} = \delta \quad \text{and} \quad d_3 = c_3 = 0 \quad \text{so that} \quad \mathcal{E} = c_0A^2+c_1AB+c_2B^2. \tag{6.4}$$

The dynamical system then takes the form

$$\frac{\mathrm{d}}{\mathrm{d}t}\begin{pmatrix} A \\ B \end{pmatrix} = \begin{pmatrix} & \mathcal{L} & \end{pmatrix}\begin{pmatrix} A \\ B \end{pmatrix} - (c_0A^2+c_1AB+c_2B^2)\begin{pmatrix} 1 & 0 \\ 0 & \delta \end{pmatrix}\begin{pmatrix} A \\ B \end{pmatrix} \tag{6.5}$$

with the additional requirements that $c_0>0$ and $4c_0c_2-c_1^2>0$ in order for $\mathcal{E}$ to be positive definite.

Despite this non-genericity, hydrodynamic systems do in fact often behave like systems of eigenvalue type. This is clear not only from the specific examples (Tuckerman 2001, Bordja *et al* 2010) treated in sections 3 and 4, but also from the many other references cited. We have seen in section 5 that the prevalence of a special class of low-dimensional dynamical systems can be explained by symmetry, either exact or weakly broken (Hirschberg and Knobloch 1997, Gallet 2011). What is needed now is an analogous theoretical framework to explain why a surprising number of hydrodynamic problems can be described so well by systems of eigenvalue type. Such a framework would presumably quantify the departure of a system from the eigenvalue type and define an appropriate projection of a system to the nearest one of eigenvalue type. Another possible avenue of research is the application of the analysis to systems other than supercritical, i.e. lifting the restrictions that $\mathcal{E}$ be a positive definite quadratic form or that $\mathcal{M}$ have positive real eigenvalues.

Short of finding, in the words of Wigner (1960), a 'rational explanation for ... the enormous usefulness of mathematics in the natural sciences ... bordering on the mysterious',

more modestly, it is likely that we will discover an explanation for the varied roles played by eigenvalues in the dynamical systems that arise in fluid dynamics.

Acknowledgments

We thank Dwight Barkley, Andrew Cliffe, Stephan Fauve, Basile Gallet, Esteban Meca, François Pétrélis and the referee for their insights and recommendations and Edgar Knobloch, Francisco Marques and Isabel Mercader for the opportunity to present this work (as well as for their insights).

References

Abshagen J, Lopez J M, Marques F and Pfister G 2005a Symmetry breaking via global bifurcations of modulated rotating waves in hydrodynamics *Phys. Rev. Lett.* **94** 074501

Abshagen J, Lopez J M, Marques F and Pfister G 2005b Mode competition of rotating waves in reflection-symmetric Taylor–Couette flow *J. Fluid Mech.* **540** 269–99

Andronov A and Leontovich E 1939 Some cases of the dependence of the limit cycles upon parameters *Uchen. Zap. Gork. Univ.* **6** 3–24

Arnold V 1982 *Geometrical Methods in the Theory of Ordinary Differential Equations* (Berlin: Springer)

Barkley D and Tuckerman L S 1989 Traveling waves in axisymmetric convection: the role of sidewall conductivity *Physica* D **37** 288–94

Barkley D, Tuckerman L S and Golubitsky M 2000 Bifurcation theory for three-dimensional flow in the wake of a circular cylinder *Phys. Rev.* E **61** 5247–52

Bergeon A, Henry D, BenHadid H and Tuckerman L S 1988 Marangoni convection in binary mixtures with Soret effect *J. Fluid Mech.* **375** 143–77

Bergeon A, Henry D and Knobloch E 2001 Three-dimensional Marangoni–Bénard flows in square and nearly square containers *Phys. Fluids* **13** 92–8

Bordja L, Tuckerman L S, Martin Witkowski L, Navarro M C, Barkley D and Bessaih R 2010a Influence of counter-rotating von Kármán flow on cylindrical Rayleigh–Bénard convection *Phys. Rev.* E **81** 036322

Bordja L, Tuckerman L S, Martin Witkowski L, Navarro M C, Barkley D and Bessaih R 2010b *Phys. Rev.* E **81** 069903 (erratum)

Da Costa L N, Knobloch E and Weiss N O 1981 Oscillations in double-diffusive convection *J. Fluid Mech.* **109** 25–43

Dumortier F, Roussarie R and Sotomayor J 1991 *Generic 3-Parameter Families of Planar Vector Fields, Unfoldings of Saddle, Focus and Elliptic Singularities with Nilpotent Linear Parts (Lecture Notes in Mathematics vol 1480)* (Berlin: Springer)

Gallet B 2011 PhD Thesis Ecole Normale Supérieure

Hirschberg P and Knobloch E 1997 Mode interactions in large aspect ratio convection *J. Nonlinear Sci.* **7** 537–56

Hollinger S, Lücke M and Müller H W 1998 Model for convection in binary liquids *Phys. Rev.* E **57** 4250–64

Knobloch E 1986 Oscillatory convection in binary mixtures *Phys. Rev.* A **34** 1538–49

Knobloch E and Guckenheimer J 1983 Convective transitions induced by a varying aspect ratio *Phys. Rev.* A **27** 408–16

Knobloch E and Proctor M R E 1981 Nonlinear periodic convection in double-diffusive systems *J. Fluid Mech.* **108** 291–316

Kumar K and Tuckerman L S 1994 Parametric instability of the interface between two fluids *J. Fluid Mech.* **279** 49–68

Kuznetsov Y 1998 *Elements of Applied Bifurcation Theory* (Berlin: Springer)

Lopez J M, Rubio A and Marques F 2006 Travelling circular waves in axisymmetric rotating convection *J. Fluid Mech.* **569** 331–48

Meca E, Mercader I, Batiste O and Ramirez-Piscina L 2004 Complex dynamics in double-diffusive donvection *Theor. Comput. Fluid Dyn.* **18** 231–8

Pétrélis F, Fauve S, Dormy E and Valet J P 2009 Simple mechanism for reversals of earth's magnetic field *Phys. Rev. Lett.* **102** 144503

Riecke H, Crawford J D and Knobloch E 1988 Time-modulated oscillatory convecction *Phys. Rev. Lett.* **61** 1942–5

Rubio A, Lopez J M and Marques F 2008 Modulated rotating convection: radially travelling concentric rolls *J. Fluid Mech.* **608** 357–78

Siggers J 2003 Dynamics of target patterns in low-Prandtl-number convection *J. Fluid Mech.* **475** 375–5
Swift J W 1984 PhD Thesis University of California at Berkeley
Swinney H L and Gollub J P 1981 *Hydrodynamic Instabilities and the Transition to Turbulence (Topics in Applied Physics vol 45)* (Berlin: Springer)
Tuckerman L S 2001 Thermosolutal and binary fluid convection as a 2×2 matrix problem *Physica* D **156** 325–63
Tuckerman L S and Barkley D 1988 Global bifurcation to travelling waves in axisymmetric convection *Phys. Rev. Lett.* **61** 408–11
Tuckerman L S and Barkley D 1990 Bifurcation analysis of the Eckhaus instability *Physica* D **46** 57–86
Wigner E P 1960 The unreasonable effectiveness of mathematics in the natural sciences *Commun. Pure Appl. Math.* **13** 1–14